Proc. Indian Acad. Sci. (Earth Planet. Sci.), Vol. 102, No. 3, September 1993, pp. 415–437.

Cosmic ray produced nitrogen in extra terrestrial matter

K J MATHEW* and S V S MURTY
Physical Research Laboratory, Ahmedabad, 380009, India
*Present address: Max-Planck Institut fur Chemie Saarstrasse 23, 55020, Mainz, Germany

MS received 16 March 1993; revised 19 August 1993

Abstract. Production rates of ^{15}N by both solar cosmic rays (SCR) and galactic cosmic rays (GCR) have been calculated for moon, as well as meteorites of various sizes. Our production rates of ^{15}N which considered both the reaction channels $^{16}O(p, pn)^{15}O$ and $^{16}O(p, 2p)^{15}N$ separately are about 30% higher than those by Reedy (1981) who considered only the channel $^{16}O(p, pn)^{15}O$ and used an empirical scaling factor to estimate the contribution from $^{16}O(p, 2p)^{15}N$. Production ratio $^{15}N/^{21}Ne$ is composition dependent and hence is different for various silicate minerals. Additionally the ratio $^{15}N/^{21}Ne$ is very sensitive to the energy spectrum of the cosmic rays. This fact can be made use of in characterizing as well as in decoupling the SCR and GCR effects in extraterrestrial samples.

Keywords. Nitrogen; neon; solar cosmic rays; galactic cosmic rays; cosmogenic nuclides; moon; meteorites.

1. Introduction

In silicate material that is exposed to cosmic rays, an isotope that is profusely produced is ^{15}N. Its principal target being oxygen, which is about 45% in common silicate minerals, ^{15}N is the most abundantly produced cosmogenic isotope, after helium. As a consequence of this, the $\delta^{15}N$ of the total nitrogen in all extraterrestrial samples are influenced by the cosmogenic ^{15}N contribution and any effort to know the $\delta^{15}N$ of the trapped N component necessitates a correction for the cosmogenic component. The importance of this correction in the derivation of the $\delta^{15}N$ signature of solar wind (implanted in the grains, prior to their compaction into the parent body) from a meteorite (Murty and Marti 1990) and the $\delta^{15}N$ signature of indigeneous lunar nitrogen (Murty and Goswami 1992) have been well documented.

Cosmogenic nitrogen in a sample can be obtained either by direct experimental measurement or through establishing a relation between ^{15}N and ^{21}Ne or ^{38}Ar (which are easily measurable), through production systematics. The former approach is only feasible in certain special achondrites like in the case of aubrites (Murty and Varun Sheel 1991) and the latter approach is the only recourse for the estimation of cosmogenic nitrogen in most extraterrestrial samples. For establishing a relation between the production rates of ^{15}N with those of ^{21}Ne and/or ^{38}Ar, the ^{15}N production systematics of Reedy (1981) which are based on limited cross section data (Audouze *et al* 1967) have been used in the past. With the recent availability of new cross section measurements, (Webber *et al* 1990; Olson *et al* 1983; Guzik *et al* 1985; Sisterson *et al* 1991) particularly from the reaction channel $^{16}O(p, 2p)^{15}N$, a re-evaluation of the ^{15}N production rates has become imperative. Also, due to the sensitivity of ^{15}N

production to low energy particles, as compared to ^{21}Ne, the production ratio $^{15}N/^{21}Ne$ will serve as a sensitive indicator to distinguish between the low energy solar cosmic ray (SCR) effects from high energy galactic cosmic ray (GCR) effects (Murty 1990). This distinction between SCR and GCR effects has become an important issue in resolving the question of the enhanced activity of ancient sun (see Caffee *et al* 1991 for a review).

2a. Theoretical approach

The theoretical model used for calculating the production rates of cosmogenic nuclides follow the procedure adopted by Reedy and Arnold (1972) for moon and further developed by Bhandari and Potdar (1982) for meteorites. The SCR production rate models used were developed by Bhattacharya *et al* (1973). The basic approach of these models is as follows. The production rate of a cosmogenic nuclide at depth d in a meteoroid of radius R (assuming the meteoroid to be spherical) can be calculated by using the expression

$$P_i(R,d) = \sum_j N_j \int_0^\infty \sigma_{ij(E)} F_{(E,R,d)} dE \tag{1}$$

N_j is the abundance of the target element j, σ_{ij} is the production cross section of nuclide i from target j and $F_{(E,R,d)}$ is the flux of cosmic ray particles as a function of energy E, meteoroid radius R and sample depth d. In case of SCR calculations, estimating the factor $F_{(E,R,d)}$ is rather straight forward as only degradation in energy of the incoming protons need to be taken into consideration and production by secondary particles is negligible. The difference in energy between the SCR and GCR particles also makes the effect that the cosmogenic production by the low energy SCR particles are confined to the surface layers of the extraterrestrial body (top 1 to 3 cms) whereas the high energy GCR particles produce nuclear interactions up to more than a meter inside the interacting body. $F_{(E,R,d)}$ is assumed to be represented by, following the Reedy and Arnold (1972) formulation,

$$F_{(E,R,d)} = k_{(R,d)}[\alpha_{(R,d)} + E]^{-2\cdot5} \tag{2}$$

where α is the spectral hardness parameter and k is the normalising constant determined by

$$k_{(R,d)} = \frac{3}{2} J_{G(>1\,\mathrm{GeV},R,d)}[\alpha_{(R,d)} + E]^{-2\cdot5} \tag{3}$$

Where J_G is the integral flux above 1 GeV. The spectral shape parameters for both meteoritic and lunar cases, used in the present calculations, are adopted from Reedy (1985). We used the same computer code, adopted by Bhandari (1988).

The fluxes of CGR particles averaged over solar cycle 20 was found to be $1{\cdot}9 \pm 0{\cdot}1$ protons/(cm^2.s.4 π sr) (Potdar and Bhandari 1979). We have used an integral flux of $J_{GCR} = 1{\cdot}8$ protons/(cm^2.s.4 π sr. 1 GeV) following Reedy (1983). In case of SCR particles an exponential rigidity of the type

$$\frac{dJ}{dR} = k\exp(-R/R_0) \tag{4}$$

was used for the proton flux. The calculations for both the meteorite and lunar situations were carried out for values of the characteristic rigidity $R_0 = 50$, 100, 150 and 200 MV.

From the methodology described above, which is used for calculating the production rates of cosmogenic nuclides in extraterrestrial matter, it becomes clear that, provided we have the cross sections for the proton and neutron induced production of the isotope at hand, from all its important cosmochemical targets for energies ranging from the threshold to about a few thousand MeV and provided the cosmic ray fluxes and energy spectra at the meteoroid and lunar orbits are available, it is possible to make sufficiently accurate estimates of the cosmogenic production rates of the given nuclide. At present only a few cross sections for neutron reactions are known. Since a large fraction of cosmogenic nuclides is produced by neutrons, the lack of knowledge of the respective cross sections is a major source of uncertainty in this type of calculation. At low energies where the excitation functions generally exhibit structures, it is important that we know the cross section values at much closer intervals. Also, since many of the secondary particles, both neutrons and protons, produced in the nuclear interactions of the primary cosmic ray particles with extraterrestrial matter are having low energies, it is essential to know separately the neutron and proton induced production cross sections of these nuclides at least up to an energy of about 50–60 MeV. Beyond this energy it is assumed that the proton and neutron induced reactions have the same cross section values (Reedy and Arnold 1972).

In the present calculations we have used the nucleon induced reaction cross sections for calculating the production rates. At very low energies, that is upto 50–60 MeV, in which region both proton and neutron induced reaction cross sections are considered separately and the excitation functions used in the present calculations are set according to which of these reaction cross sections is higher. The shape of the excitation function is also decided according to the shape of the major reaction channel, independent of whether it is neutron or proton induced. As far as the proton induced reactions are concerned significant work has been carried out in the last decade and the excitation functions for the proton induced reactions leading to production of nitrogen and neon isotopes can be determined sufficiently accurately using the available cross section measurements. The recent neutron cross section measurements (Lavielle *et al* 1990; Leich *et al* 1984; Reedy *et al* 1979) for the production of ^{21}Ne have been incorporated in our calculations.

2b. Experimental approach

The experimental determination of the cosmogenic nitrogen amounts in a meteorite or lunar sample is rather difficult. The total nitrogen in such a sample is a mixture of trapped and cosmic ray produced components. The trapped nitrogen in a meteorite will be several ppm while the cosmogenic component seldom exceeds few hundred ppt. But the $^{15}N/^{14}N$ of the cosmogenic component is so high compared to the trapped component, it contributes significantly to the total $\delta^{15}N$ of the sample. Hence, if the composition of the trapped component is known, the cosmogenic amounts can be estimated. In the case of most meteorites (except aubrites) the composition of the trapped component is not known precisely and hence it is not possible to accurately determine the cosmogenic amounts. In aubrites, the composition of the

trapped nitrogen is relatively well established (Grady *et al* 1986). Hence measurement of the nitrogen in these meteorites can yield the cosmogenic nitrogen amounts.

3. Excitation functions

Oxygen, by its proximity to the nitrogen isotopes in the table of nuclides, is the most important target for the production of these isotopes. As a result of the irradiation experiments by Webber *et al* (1990), Olson *et al* (1983), Guzik *et al* (1985) and Sisterson *et al* (1991) the production cross sections for nitrogen isotopes are available over most of the energy regions representative of the SCR and GCR particles. For a compilation of the production cross sections of light nuclei from light targets see Read and Viola (1984).

In addition, for those energy regions where experimental cross section determinations are not carried out so far, some valid assumptions can be made about the excitation functions based on the knowledge of the general systematics of particle induced reactions. The general shapes of the excitation functions of ^{15}O and ^{14}O can thus be assumed based on the excitation functions for the analogous reactions for the production of ^{11}B and ^{10}B from target ^{12}C. ^{15}O is produced from ^{16}O by (p, pn) reaction and ^{11}B is produced from ^{12}C by (p, pn) reaction. Similarly $(p, p2n)$ reactions on targets ^{16}O and ^{12}C produce isotopes ^{14}O and ^{10}B. Further, in all the above cases the masses of the targets and the mass difference between the target and product nucleus are similar and hence these reactions can be assumed as following a similar course.

Figure 1(a) shows the excitation functions of isotopes ^{15}N and ^{15}O (which decays to ^{15}N) from oxygen target. For the reaction $^{16}O(p, pn)^{15}O$ measured cross section values are available for energies as low as 25 MeV. The excitation functions below 25 MeV for this isotope is determined by extrapolating the curve to still lower energies and making use of the fact that the threshold energy for this reaction is 16 MeV. In the case of the direct production through channel $^{16}O(p, 2p)^{15}N$ the lowest energy at which cross-section measurements are available is 55 MeV. The production cross sections of this reaction for energies lower than 55 MeV are deduced based on the isobaric yields ($^{15}O + ^{15}N$) deduced by Guzik *et al* (1985) and the known excitations function of ^{15}O.

Figure 1(b) shows the excitation functions for isotopes ^{14}N and ^{14}O (the latter nuclide decaying to ^{14}N) from oxygen targets. The production cross sections for the isotope ^{14}C, which is produced by the reaction $^{16}O(p, 3p)^{14}C$, is relatively small (around 2 to 4 mb) at all energies. The production of ^{14}N from the decay of ^{14}C are included in the present calculations though the excitation functions for this reaction are not shown in figure 1(b). The excitation functions for ^{14}O production are reconstructed such that the shape of this excitation function resembles that of the analogous reaction $^{12}C(p, p2n)^{10}B$. As in the previous case the excitation function for ^{14}N is determined from the isobaric yields of mass 14, given by Guzik *et al* (1985) and the excitation function of ^{14}O.

In case of neon isotopes the cross section measurements, from its various targets, are numerous and the excitation function for the proton induced production of ^{21}Ne from the targets Mg, Si, Al and Na are known sufficiently accurately. The excitation functions for isotope ^{21}Ne used in the present calculations incorporate the results of the recent cross section measurements by Lavielle *et al* (1990), Webber *et al* (1983), Baros and Regnier (1984) and Leich *et al* (1984).

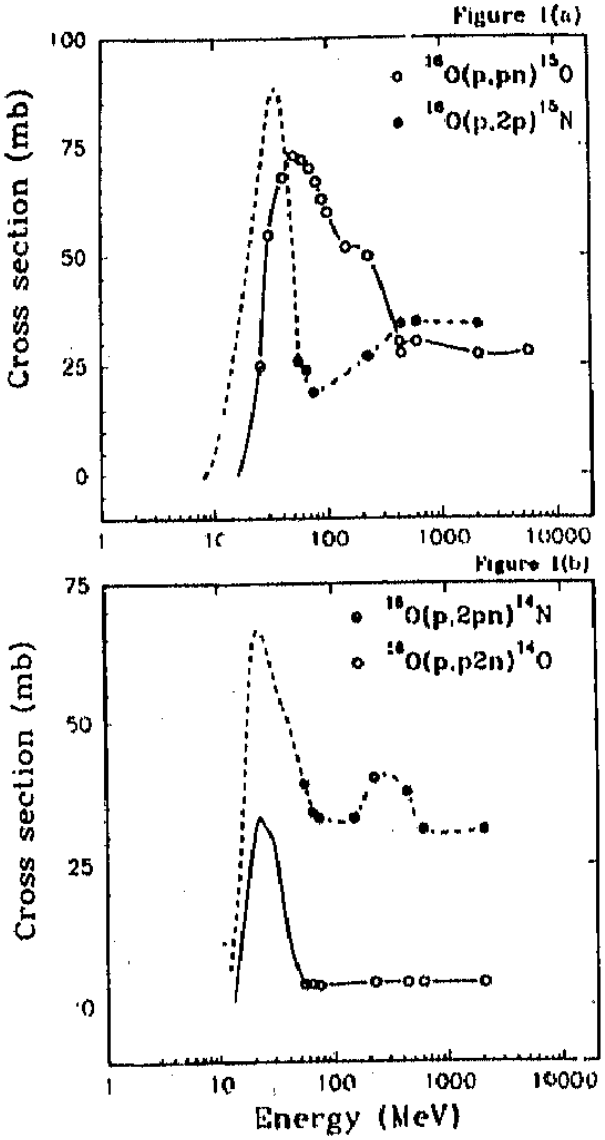

Figure 1. Excitation functions of (a) $^{16}O(p,pn)^{15}O$ and $^{16}O(p,2p)^{15}N$, (b) $^{16}O(p,p2n)^{14}O$ and $^{16}O(p,2pn)^{14}N$.

4. Results and discussions

In the following discussion the results of the production rate calculations for the case of moon (size of the interacting body much much larger than the mean free path of the high energy cosmic ray particles) are dealt with first and the meteoritic calculations are taken up later. Further we will concentrate the discussion around the production rates of isotopes ^{15}N and ^{21}Ne.

4.1 *GCR production rates of nitrogen and neon isotopes on the lunar surface*

Table 1 shows the production rates of nitrogen and neon isotopes from pure target elements as a function of shielding depth. In case of GCR particles, the direct ^{15}N production rates at all shielding depths, from 0·0 g/cm^2 to 500 g/cm^2 are lower than the contribution from the indirect production through ^{15}O. For example the surface

Table 1. Production rates of nitrogen and neon isotopes from pure target elements as a function of shielding depth on the lunar surface material. These calculations are carried out for a GCR flux of 1·8 protons/cm^2/s.

Shielding depth g/cm^2	^{14}N atoms/min/kg	^{15}N atoms/min/kg			^{21}Ne atoms/min/kg			
		^{15}N	^{15}O	Total	Mg	Al	Si	Na
0	407	343	425	768	296	131	74	121
5	434	364	449	813	320	135	75	136
10	490	409	503	912	384	145	79	151
20	535	444	543	987	445	150	80	166
40	582	482	583	1065	522	152	78	181
65	555	456	550	1006	519	137	70	166
100	498	411	486	897	487	117	58	151
225	304	251	289	540	326	62	29	91
350	155	129	143	272	174	29	13	48
500	53	45	49	94	61	10	4·1	17

production rates (in units atoms/min/kg target) of ^{15}N and ^{15}O are, respectively 343 and 425. At a shielding depth of 40 g/cm^2, where the production rates are maximum due to development of the secondary protons and neutrons within the interacting body, the ^{15}N and ^{15}O productions are 482 and 583 atoms/min/kg target. At still higher depths also the ^{15}O production rates remain higher than the ^{15}N production rates.

The ^{21}Ne production rates calculated here, for the lunar irradiation conditions, can be compared with those estimated by Hohenberg *et al* (1978). Hohenberg *et al* (1978) estimated the production rates of ^{21}Ne in lunar surface samples from the targets Mg, Al, Si and Na, separately. The ^{21}Ne production rates in any mineral can be obtained from these elemental production rates by multiplying them with the target element abundance and summing over all the targets. Figures 2(a) and 2(b) show a comparison of the ^{21}Ne production rates estimated by us with those calculated by Hohenberg *et al* (1978) for minerals olivine and feldspar (figure 2(a)) and orthopyroxene and clinopyroxene (figure 2(b)). This comparison shows that the production rates estimated by us are in good agreement with those by Hohenberg *et al* (1978). It may be more appropriate to compare our ^{21}Ne production rates with those of Bhandari (1988) as we used the same computer code. But we only have one common datum i.e. a sample at 20 g/cm^2 depth in a body of infinite size. Our values match with those of Bhandari (1988) for all the four minerals within 10%. It might be mentioned here that our excitation functions include some recent cross section data.

As has been mentioned already the ^{15}O production rates, calculated above, can be compared with the production rates obtained by Reedy (1981). For the calculation of ^{15}N production rates in a silicate sample, we only consider oxygen (which makes up about 45% of all silicates) as the target element. ^{15}N production from other major elements in silicates (Mg, Al, Si and Fe) is negligible compared to the production from oxygen. For example, in the case of olivine, it can be shown that the ^{15}N production from Mg, Al and Si is only 2 to 3% of that due to O, making use of the target-product systematics of Honda (1988). So for all practical purposes, the production from O will represent the total ^{15}N produced in silicate minerals. Figure 3(a) shows

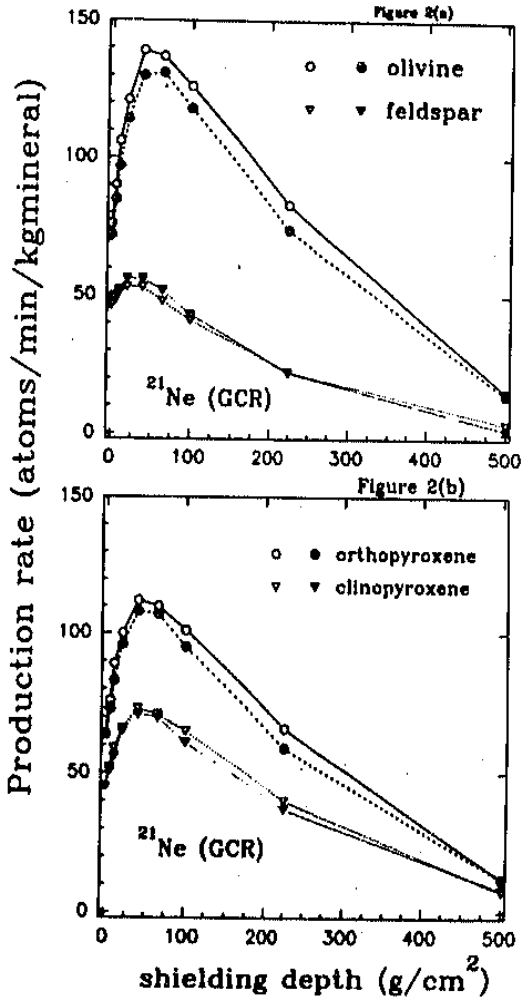

Figure 2. Comparison of GCR produced ^{21}Ne production rates with those of Hohenberg *et al* (1978) (a) olivine and feldspar, (b) orthopyroxene and clinopyroxene.

a comparison of our data with that of Reedy (1981) for a silicate mineral (O = 45%). Here it has to be remembered that the total ^{15}N production rates are obtained by Reedy by suitably scaling the ^{15}O production. Only the production rates of ^{15}O are calculated by Reedy (1981) using the cross-section data of Audouze *et al* (1967). The ^{15}O production rates were then compared with measured estimates of the ^{15}N production rates by Becker *et al* (1976) to derive an appropriate scaling factor to convert cosmogenic ^{15}O production rate into ^{15}N (total). By this comparison it was concluded that the contribution of the $^{16}O(p,2p)^{15}N$ channel in the total production rate of ^{15}N is 30%. But the assumptions on which Becker *et al* (1976) obtained the cosmogenic ^{15}N have some shortcomings. Becker *et al* (1976) deduced ^{15}N production rate of 275 atoms/min/kg sample by assuming that cosmogenic nitrogen is released only at high temperatures ($\geqslant$ 1200°C). However a part of the cosmogenic nitrogen in an extraterrestrial sample can be released at lower temperatures also leading to an underestimation of $^{15}N_c$. Figure 3(b) shows a comparison of the total ^{15}N production rates (sum of the ^{15}O and ^{15}N yields) obtained in the present study with the ^{15}O production rates by Reedy (1981) scaled up to obtain the total ^{15}N. Our ^{15}O production rates are in good agreement with those of Reedy (1981) but our total ^{15}N

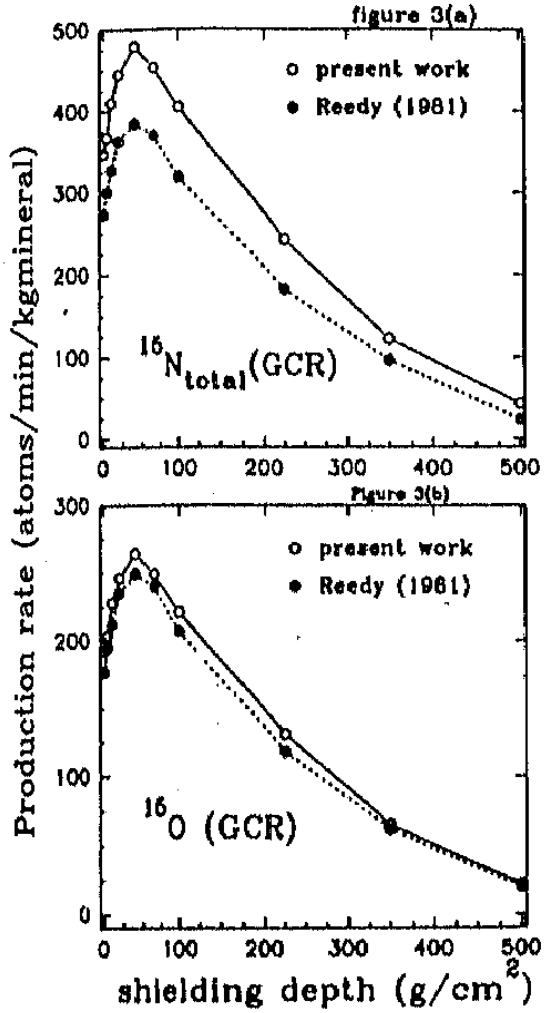

Figure 3. Comparison of GCR produced production rates with those of Reedy (1981) (a) ^{15}N (total), (b) ^{15}O.

production rates are 30% higher. This is due to an underestimation of the direct production of ^{15}N by Reedy (1981). Shapiro and Silberberg (1970) deduced the $^{13}C/^{15}N$ production ratio from oxygen to be in the range of 0·40 to 0·48 for protons with E = 150 and ⩾2300 MeV respectively. Estimates by Reedy (1981) for $^{13}C/^{15}N$(^{13}C = total production of ^{13}C from all channels, $^{15}N = {}^{15}O \times 1{\cdot}55$) range from 0·68 to 1·38. This discrepancy can be understood as due to an underestimation of the direct production of ^{15}N by Reedy (1981) and supports the higher ^{15}N (total) production rates obtained in the present work.

In sharp contradiction to the neon isotopes, where the target element abundances, (Mg, Al, Si and Na) vary over a wide range from mineral to mineral and from meteorite of one kind to another, the abundance of the target for the production of nitrogen isotopes, viz oxygen, is almost the same in all commonly occurring silicate material. These variations in the target element abundance will be reflected in the cosmic ray produced $^{15}N/^{21}Ne$ ratio. Below we discuss the variation in the cosmogenic $^{15}N/^{21}Ne$ ratio.

Table 3 shows the isotopic production rates obtained by us for minerals with composition (Allen and Mason 1973) given in table 2. For the case of an olivine

Table 2. Elemental composition of the targets for production of nitrogen and neon, used in the present calculations (in % units)

Element	Olivine	Feldspar	O. Pyroxene	C. Pyroxene	H	L
O	45·0	45·0	45·0	45·0	35·7	37·7
Mg	23·9	0·04	17·7	10·1	14·2	15·2
Al	0·01	11·0	0·06	0·3	1·01	1·1
Si	17·8	30·5	26·0	25·3	17·1	18·7
Na	0·02	7·0	0·03	0·43	0·57	0·65

Table 3. Production rates of nitrogen and neon isotopes in olivine, feldspar, orthopyroxene and clinopyroxene mineral as a function of shielding depth in a lunar sized body. These calculations are carried out for a GCR flux of 1·8 protons/cm^{-2}/s^{-1}.

Shielding depth g/cm^2	^{15}N atoms/min/kg	^{14}N/^{15}N	^{21}Ne atoms/min/kg				^{15}N/^{21}Ne			
			oliv	fels	opyx	cpyx	oliv	fels	opyx	cpyx
0	347	0·530	76	46	64	45	4·60	7·54	5·42	7·71
5	367	0·529	90	48	76	52	4·08	7·65	4·83	7·06
10	410	0·537	106	51	89	59	3·87	8·04	4·61	6·95
20	445	0·542	121	53	100	66	3·68	8·40	4·45	6·74
40	479	0·545	139	53	112	73	3·45	9·04	4·28	6·56
65	454	0·551	137	48	110	71	3·31	9·46	4·13	6·39
100	405	0·556	126	41	101	65	3·21	9·88	4·01	6·23
225	243	0·564	83	22·3	66	40	2·93	10·90	3·68	6·08
350	122	0·574	43	10·8	34	21	2·84	11·30	3·59	5·81
500	43	0·581	15	3·4	12	7·4	2·87	12·70	3·58	5·81

mineral in a body of large size the ^{15}N/^{21}Ne ratio decreases by 38% between the surface and a shielding depth of 500 g/cm^2. Corresponding to a shielding depth of 0 g/cm^2 the ^{15}N/^{21}Ne ratio is 4·6 and the value at shielding depth 500 g/cm^2 is 2·9. In the case of feldspar mineral the ^{15}N/^{21}Ne ratio increases with shielding depth and the increase is by as much as 60% between the surface and a shielding depth of 500 g/cm^2. In case of orthopyroxene or clinopyroxene the changes in ^{15}N/^{21}Ne ratios for the same shielding depths are 34% and 25%, respectively. Since the oxygen abundance is ~45% for all the minerals considered here, the differences in the depth profiles of ^{15}N/^{21}Ne for various minerals are strictly controlled by the ^{21}Ne production rate alone. For olivine and pyroxenes the ^{21}Ne production profile is mainly controlled by the element Mg, whereas for feldspar the chief controlling elements are Al and Si. For this reason the depth profiles of ^{15}N/^{21}Ne for olivine and pyroxene are similar, whereas that of feldspar is different. Also the ^{21}Ne production from Mg increases very steeply with depth while for Al and Si the increase with depth is not very pronounced. On the other hand the ^{15}N production profile is intermediate to the above two trends. These characteristics result in the decreasing trend of ^{15}N/^{21}Ne with depth for olivine and pyroxenes and in an increasing trend for the case of feldspar. Figure 4(a) and 4(b) show the variations in ^{15}N/^{21}Ne ratios as a function of shielding depth in a lunar sized body and for all the four minerals mentioned above.

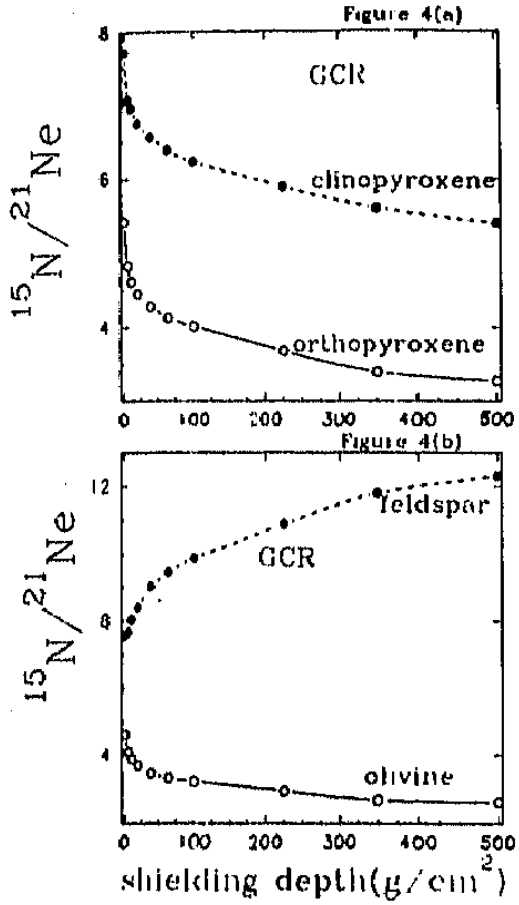

Figure 4. $^{15}N/^{21}Ne$ as a function of shielding depth (a) in minerals olivine and feldspar, (b) in minerals orthopyroxene and clinopyroxene.

4.2 *SCR production rates of nitrogen and neon isotopes on the lunar surface*

Tables 4 and 5 show the results of the SCR production rate calculations of the nitrogen and neon isotopes for minerals olivine, feldspar, orthopyroxene and clinopyroxene, for an SCR spectrum with characteristic rigidity of 100 MV (and 200 MV) and for integral flux of SCR particles (> 10 MeV) = 100 protons/cm^2/s. The combination of (J_0, R_0) of (100, 100) closely corresponds to the contemporary Sun as recently shown by Rao *et al* (1993). For the case of 'Early Sun' the possibility of having a harder energy spectrum cannot be ruled out. For this reason we also included a set of production rates for the case of $R_0 = 200$ MV as well. From these tables it becomes clear that the SCR production is confined to the top few g/cm^2 of the lunar surface material, the production rate exponentially decreasing as the shielding depth increases. The surface production rate of ^{15}N is 3429 atoms/min/kg mineral (assumed oxygen abundance is 45%). At a shielding depth of 1 g/cm^2 the SCR production rate of ^{15}N decreases to 970 atoms/min/kg mineral and at a shielding depth of 20 g/cm^2 it becomes 26 atoms/min/kg mineral.

Figure 5(a) shows a comparison of the ^{15}O SCR production rate obtained by us with those by Reedy (1981) and figure 5(b) shows a comparison of the SCR production rates of ^{15}N (total) obtained here as against the Reedy's ^{15}O production rates scaled up by a factor of 1·55 to obtain the ^{15}N production rates. The ^{15}O production rates

Table 4. Production rates of nitrogen and neon isotopes in olivine, feldspar, orthopyroxene and clinopyroxene mineral as a function of shielding depth in a lunar sized body. These calculations are carried out for an SCR flux of 100 protons/cm^{-2}/s^{-1} and for a characteristic rigidity of 100 MV.

Shielding depth g/cm^2	^{15}N atoms/min/kg	^{14}N/^{15}N	^{21}Ne atoms/min/kg				^{15}N/^{21}Ne			
			oliv	fels	opyx	cpyx	oliv	fels	opyx	cpyx
0·00	3429	0·653	531	179	411	249	6·46	19·2	8·3	13·8
0·10	2533	0·621	368	144	287	177	6·88	17·6	8·8	14·3
0·33	1787	0·588	250	110	196	122	7·15	16·2	9·1	14·6
0·50	1470	0·571	204	95	161	101	7·21	15·5	9·1	14·6
1·00	970	0·542	135	68	108	68	7·18	14·3	9·0	14·3
2·00	558	0·516	80	44	64	42	6·98	12·7	8·7	13·3
5·00	211	0·493	32	19	27	18	6·59	11·1	7·8	11·7
10·00	82	0·488	14	8·6	12	8	5·86	9·5	6·8	10·3
20·00	26	0·500	5	3·1	4	3	5·2	8·4	6·5	8·7

Table 5. Production rates of nitrogen and neon isotopes in olivine, feldspar, orthopyroxene and clinopyroxene mineral as a function of shielding depth in a lunar sized body. These calculations are carried out for an SCR flux of 100 protons/cm^{-2}/s^{-1} and for a characteristic rigidity of 200 MV.

Shielding depth g/cm^2	^{15}N atoms/min/kg	^{14}N/^{15}N	^{21}Ne atoms/min/kg				^{15}N/^{21}Ne			
			oliv	fels	opyx	cpyx	oliv	fels	opyx	cpyx
0·00	3933	0·580	605	298	488	313	6·50	13·2	8·1	12·6
0·10	3285	0·559	498	267	405	264	6·60	12·3	8·1	12·4
0·33	2671	0·539	406	233	334	220	6·58	11·5	8·0	12·1
0·50	2380	0·531	364	215	301	199	6·54	11·1	7·9	12·0
1·00	1874	0·518	294	183	245	165	6·37	10·2	7·7	11·4
2·00	1366	0·509	222	146	188	128	6·15	9·4	7·3	10·7
5·00	789	0·508	137	96	118	82	5·76	8·2	6·7	9·6
10·00	468	0·517	86	63	75	53	5·44	7·4	6·2	8·8
20·00	250	0·528	47	37	43	31	5·3	6·8	5·8	8·1
40·00	118	0·542	24	19	22	16	4·9	6·2	5·4	7·4

obtained in these two studies agree reasonably well with each other whereas the ^{15}N total (sum of the ^{15}N and ^{15}O production in the present case and the ^{15}O production rates multiplied by the scaling factor of 1·55 in the case of Reedy 1981) are significantly different from each other. For example the surface production rates obtained in these two studies are 3429 and 2189 (in units atoms/min/kg). These differences become less significant at higher shielding depths. At a shielding depth of 0·7 g/cm^2 the production rate obtained by us are 1223 atoms/min/kg as compared to 1046 (in same units) estimated by Reedy (1981). Here the scaling factor 1·55 is used to convert Reedy's ^{15}O production rates to ^{15}N (total), assuming that the relative production of ^{15}O and ^{15}N (direct) will be the same in both low and high energy region, which may not be correct. But in the absence of any experimental data on SCR produced $^{15}N_{c}$, this is our best choice. The higher SCR production rates obtained here are consistent

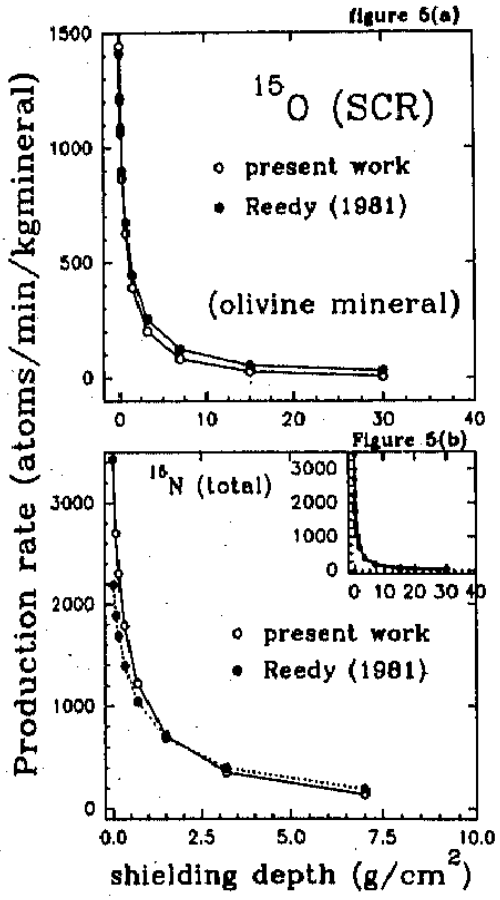

Figure 5. Comparison of SCR production rates (a) for ^{15}O, (b) for ^{15}N (total) with Reedy (1981).

with the shapes of the excitation functions for the (p, pn) and $(p, 2p)$ channels in the low energy region that is important for SCR.

Figure 6 shows a comparison of the ^{21}Ne production rates obtained by us with those of Reedy (1992). Reedy's elemental production rates were multiplied with the elemental abundances of the targets in olivine mineral to obtain the production rates plotted here. The production rates calculated by Reedy (1992) are slightly higher than those estimated by us, but these differences are within the uncertainties of the calculational method.

Here also, as in the case of GCR induced production of nitrogen and neon isotopes, the ^{15}N/^{21}Ne ratio changes from one mineral to another and with shielding depth in the same mineral. These variations are much steeper in comparison with the GCR production rate ratios. Figure 7(a) shows the variations in the ^{15}N/^{21}Ne ratio with shielding depth for minerals olivine, feldspar, orthopyroxene and clinopyroxene. Considering the case of olivine mineral the surface value of ^{15}N/^{21}Ne ratio and that at a shielding depth of 20 g/cm^2 are, respectively, 6·5 and 5·2. In case of feldspar mineral there is a difference in the variation of the ^{15}N/^{21}Ne ratio with regard to the GCR and SCR production. For GCR production this ratio increases with increasing shielding depth whereas for the case of SCR production the ^{15}N/^{21}Ne ratio decreases with shielding depth. The SCR depth profiles for both ^{15}N and ^{21}Ne decrease steeply with depth due to the steep decrease in the proton flux with depth (Reedy

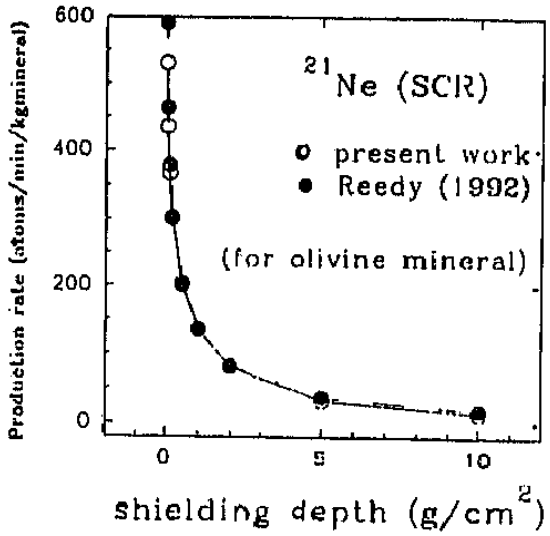

Figure 6. Comparison of SCR produced ^{21}Ne in mineral olivine with Reedy (1992).

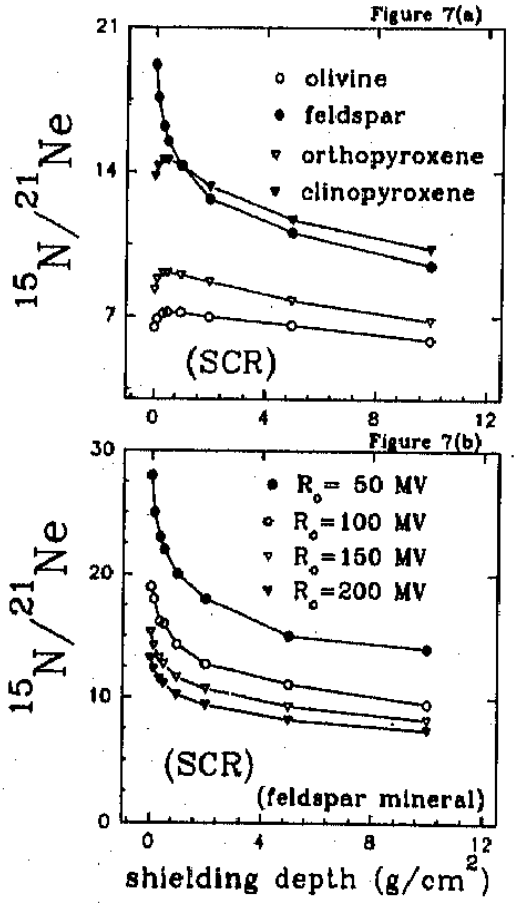

Figure 7(a). ^{15}N/^{21}Ne (SCR) as a function of shielding depth in minerals olivine, feldspar, orthopyroxene and clinopyroxene (R_0 = 100 MV, J_0 = 100 p/cm^{2}sec) (b) ^{15}N/^{21}Ne (SCR) in mineral feldspar as a function of shielding depth for an SCR spectra with different rigidities.

Table 6. Production rates of nitrogen and neon isotopes in olivine, feldspar, orthopyroxene and clinopyroxene mineral as a function of shielding depth in meteoroids. These calculations are carried out for a GCR flux of 2·3 protons/cm^{-2}/s^{-1}.

Shielding depth g/cm^2	^{15}N atoms/min/kg	^{14}N/^{15}N	^{21}Ne atoms/min/kg			^{15}N/^{21}Ne		
			oliv	fels	opyx	oliv	fels	opyx
$R = 18$ g/cm^2								
0·00	681	0·524	160	94	151	4·3	7·2	4·5
1·80	690	0·523	163	94	153	4·2	7·3	4·5
3·60	708	0·526	165	97	154	4·3	7·3	4·6
5·40	731	0·528	167	97	156	4·4	7·6	4·7
7·20	759	0·524	169	101	157	4·5	7·5	4·8
9·00	771	0·525	170	104	159	4·5	7·4	4·8
10·8	787	0·526	172	104	160	4·6	7·6	4·9
12·6	798	0·527	175	104	162	4·6	7·7	4·9
14·4	819	0·528	177	106	164	4·6	7·7	5·0
18·0	839	0·529	179	110	167	4·7	7·6	5·0
$R = 36$ g/cm^2								
0·00	688	0·525	152	94	148	4·5	7·3	4·6
3·60	741	0·525	161	99	156	4·6	7·7	4·8
7·20	796	0·529	173	104	163	4·6	7·7	4·9
10·8	833	0·530	185	108	172	4·5	7·9	4·7
14·4	872	0·530	194	110	180	4·5	7·9	4·8
18·0	890	0·532	206	113	186	4·3	7·9	4·8
21·6	918	0·531	225	115	191	4·1	8·0	4·8
28·8	968	0·534	242	120	205	4·0	8·1	4·7
32·4	991	0·534	251	124	209	4·0	8·0	4·7
36·0	991	0·534	251	124	209	4·0	8·0	4·7
$R = 72$ g/cm^2								
0·00	736	0·528	161	99	150	4·6	7·4	4·9
7·20	872	0·533	214	110	182	4·1	7·9	4·8
14·4	938	0·534	237	115	198	4·0	8·2	4·7
21·6	991	0·536	258	120	214	3·8	8·3	4·6
28·8	1040	0·538	274	124	228	3·8	8·3	4·6
36·0	1095	0·540	292	131	248	3·7	8·4	4·5
43·2	1116	0·540	301	131	248	3·7	8·4	4·5
57·6	1155	0·542	315	136	260	3·7	8·5	4·4
64·8	1162	0·541	317	136	262	3·7	8·5	4·4
72·0	1159	0·542	317	136	262	3·7	8·5	4·4
$R = 108$ g/cm^2								
0·00	690	0·527	132	90	126	5·2	7·7	5·5
3·00	697	0·528	141	90	133	4·9	7·8	5,2
10·8	711	0·531	156	90	141	4·6	7·9	5·0
18·0	734	0·533	179	92	152	4·1	7·9	4·8
28·8	773	0·533	193	97	163	4·0	8·0	4·7
36·0	814	0·534	209	101	175	3·9	8·0	4·7
45·0	860	0·537	225	104	189	3·8	8·3	4·4
64·8	961	0·541	262	113	216	3·7	8·5	4·4
72·0	1001	0·543	276	115	225	3·6	8·7	4·4
108·0	1086	0·544	306	122	251	3·6	8·9	4·3

(Continued)

Table 6. (*Continued*)

Shielding depth g/cm²	^{15}N atoms/min/kg	$^{14}N/^{15}N$	^{21}Ne atoms/min/kg			$^{15}N/^{21}Ne$		
			oliv	fels	opyx	oliv	fels	opyx
$R = 180$ g/cm²								
0·00	626	0·529	127	83	116	4·9	7·6	5·4
7·20	635	0·530	136	83	127	4·7	7·7	5·0
14·4	649	0·532	159	83	136	4·1	7·8	4·8
36·0	727	0·538	189	87	159	3·9	8·3	4·6
43·2	754	0·537	200	90	173	3·8	8·4	4·5
72·0	842	0·544	237	94	193	3·6	8·9	4·4
90·0	860	0·546	242	96	195	3·5	8·9	4·3
108·0	904	0·547	262	99	214	3·4	9·1	4·2
144·0	881	0·548	258	97	209	3·4	9·1	4·2
180·0	863	0·547	253	94	205	3·4	9·1	4·2
$R = 360$ g/cm²								
0·00	545	0·527	120	71	112	4·5	7·6	4·9
14·4	607	0·534	154	76	129	3·9	8·0	4·7
36·0	662	0·538	179	78	147	3·7	8·5	4·5
72·0	727	0·547	212	81	173	3·4	9·0	4·2
86·4	771	0·549	232	83	186	3·3	9·3	4·1
144·0	830	0·557	267	83	212	3·1	10·0	3·9
180·0	897	0·559	297	87	235	3·0	10·3	3·8
288·0	849	0·564	290	78	228	2·9	10·9	3·7
360·0	789	0·566	271	74	212	2·9	10·7	3·7

R = Size of the body.

and Arnold 1972). Here again the different behaviour of $^{15}N/^{21}Ne$ in feldspar versus the other minerals is solely due to the ^{21}Ne production profile (controlled by Mg in olivine/pyroxenes and Al, Si in feldspar respectively). The steepness of the depth profile for the minerals olivine and pyroxenes is very similar but is more compared to that of the mineral feldspar. The steepness of the ^{15}N depth profile is in between those of ^{21}Ne profile for olivine/pyroxenes and feldspar. These facts explain the similarity in the SCR $^{15}N/^{21}Ne$ depth profiles of olivine and pyroxenes and their difference with feldspar. Also the differences in the steepness of ^{21}Ne depth profiles account for the opposing trends in olivine/pyroxenes on the one hand and feldspar on the other. The zero shielding depth value of $^{15}N/^{21}Ne$ production ratio for feldspar mineral is 7·6 and 19·2 for the GCR and SCR particles respectively. At 5 g/cm² the corresponding values are 7·7 and 11·1. As the shielding depth increases further the GCR $^{15}N/^{21}Ne$ production rate ratio continues to increase while the SCR value of this ratio decreases and both become 8·4 at 20 g/cm².

As the characteristic rigidity of the SCR spectrum is increased to 200 MV the absolute productions increase in the case of all isotopes. Further the relative yields tend toward the corresponding GCR values. In the case of feldspar mineral, figure 7(b)

Table 7. Production rates of nitrogen and neon isotopes in H and L chondrite as a function of shielding depth. These calculations are carried out for a GCR flux of 2·3 protons/cm^{-2}/s^{-1}.

Shielding depth g/cm^2	^{15}N atoms/min/kg		^{14}N/^{15}N		^{21}Ne atoms/min/kg		^{15}N/^{21}Ne	
	H	L	H	L	H	L	H	L
				$R = 18$ g/cm^2				
0·00	541	570	0·520	0·520	122	131	4·4	4·4
1·80	547	577	0·530	0·530	122	132	4·5	4·4
3·60	561	593	0·520	0·530	125	135	4·5	4·4
5·40	580	614	0·530	0·520	127	137	4·6	4·5
7·20	603	637	0·530	0·520	129	139	4·7	4·6
9·00	612	646	0·530	0·530	132	142	4·6	4·5
10·8	623	656	0·530	0·530	135	145	4·6	4·5
14·4	651	688	0·530	0·530	138	147	4·7	4·7
18·0	667	704	0·530	0·530	142	150	4·7	4·7
				$R = 36$ g/cm^2				
0·00	545	577	0·53	0·53	115	125	4·7	4·6
3·60	587	621	0·53	0·53	119	129	4·9	4·8
7·20	636	667	0·53	0·53	124	132	5·1	5·1
10·8	662	699	0·53	0·53	129	137	5·1	5·1
14·4	692	731	0·53	0·53	133	145	5·2	5·0
18·0	706	745	0·53	0·53	140	151	5·0	4·9
21·6	727	768	0·53	0·53	150	161	4·8	4·8
28·8	768	812	0·53	0·53	161	173	4·8	4·7
32·4	787	830	0·54	0·53	166	177	4·7	4·7
36·0	787	830	0·54	0·53	166	177	4·7	4·7
				$R = 72$ g/cm^2				
0·00	584	616	0·53	0·53	108	116	5·4	5·3
7·20	692	731	0·53	0·53	143	152	4·9	4·8
14·4	743	787	0·54	0·54	156	168	4·8	4·7
21·6	787	830	0·54	0·54	168	182	4·7	4·6
28·8	826	872	0·54	0·54	179	193	4·6	4·5
36·0	869	918	0·54	0·54	191	205	4·6	4·5
43·2	886	936	0·54	0·54	196	209	4·5	4·5
57·6	915	966	0·54	0·54	205	219	4·5	4·4
64·8	922	973	0·54	0·54	207	221	4·5	4·4
72·0	920	973	0·54	0·54	205	221	4·5	4·4
				$R = 108$ g/cm^2				
0·00	547	580	0·53	0·53	100	108	5·5	5·4
3·60	552	582	0·53	0·53	104	112	5·2	5·2
10·8	564	596	0·53	0·53	110	119	5·1	5·0
18·0	582	614	0·53	0·53	120	129	4·9	4·8
28·8	612	646	0·53	0·53	129	138	4·8	4·7
36·0	646	681	0·53	0·54	138	147	4·7	4·6
45·0	683	722	0·54	0·54	147	159	4·6	4·6
64·8	764	805	0·54	0·54	170	182	4·5	4·4
72·0	794	837	0·54	0·54	177	191	4·5	4·4
108·0	863	909	0·54	0·57	198	212	4·4	4·3

(*Continued*)

Table 7. (*Continued*)

Shielding depth g/cm²	^{15}N atoms/min/kg		$^{14}N/^{15}N$		^{21}Ne atoms/min/kg		$^{15}N/^{21}Ne$	
	H	L	H	L	H	L	H	L
			$R = 180$ g/cm²					
0·00	497	527	0·53	0·53	108	112	4·6	4·7
7·20	504	534	0·53	0·53	112	118	4·5	4·5
14·4	515	545	0·53	0·53	118	124	4·4	4·4
36·0	575	607	0·54	0·54	124	133	4·6	4·6
43·2	598	630	0·54	0·54	131	140	4·6	4·5
72·0	669	706	0·54	0·54	152	163	4·4	4·3
90·0	651	688	0·54	0·55	150	161	4·4	4·3
108·0	715	757	0·55	0·55	168	182	4·3	4·2
144·0	699	738	0·55	0·55	166	177	4·2	4·2
180·0	683	722	0·55	0·55	161	175	4·2	4·1
			$R = 360$ g/cm²					
0·00	432	458	0·53	0·53	85	89	5·1	5·2
14·4	481	508	0·54	0·53	101	108	4·8	4·7
36·0	524	554	0·54	0·54	117	124	4·5	4·5
72·0	577	610	0·55	0·55	136	145	4·3	4·2
86·4	612	646	0·55	0·55	147	159	3·9	3·9
144·0	658	695	0·56	0·56	168	179	3·8	3·8
180·0	711	752	0·56	0·56	186	200	3·8	3·8
216·0	725	764	0·56	0·56	193	207	3·7	3·6
288·0	674	711	0·56	0·56	182	196	3·7	3·6
360·0	626	662	0·57	0·56	168	182	3·7	3·6

R = Size of the body.

shows the variation in the $^{15}N/^{21}Ne$ ratio as a function of shielding depth on the lunar surface for different assumed characteristic rigidities. At values of SCR characteristic rigidity less than 100 MV the absolute production rates decrease substantially and the differences in the $^{15}N/^{21}Ne$ ratios also become more pronounced.

The change is the largest for feldspar mineral. If the SCR spectrum assumed has a characteristic rigidity of 50 MV the $^{15}N/^{21}Ne$ value at zero shielding depth on the lunar surface is 28. As the SCR spectrum becomes harder, as the characteristic rigidity approaches a value of 100 MV, the surface value of $^{15}N/^{21}Ne$ becomes 19 and for still higher R_0 values the $^{15}N/^{21}Ne$ ratio further reduced to 15 at 150 MV and 13 at 200 MV. These variations can be made use of in determining the characteristic rigidity of SCR spectrum by the measurement of the cosmogenic nitrogen and neon isotopes in well documented lunar rock samples.

4.3 *GCR production of nitrogen and neon isotopes in meteorites*

Considering the irradiation of meteorites in space to the energetic GCR and SCR particles a major difference from the lunar situation is that since the size of these bodies are small they receive 4π isotropic irradiation. Further, the flux of these radiations

gets altered as the distance from the sun increases. The GCR flux is estimated to increase by 2–3% per A.U. distance from the sun (McKibben *et al* 1982). For the meteorite calculations here we have used an integral flux $J_{GCR>GeV} = 2{\cdot}3$ protons/cm^2/s following Michel *et al* (1991).

The target element abundances used in the present calculations for the various minerals and also for the H and L chondrites are shown in table 2. In the present calculations we have estimated the production rates of isotopes ^{14}N, ^{15}N and ^{21}Ne for meteorite bodies having size 5 cm, 10 cm, 20 cm, 30 cm, 50 cm and 100 cm and for the minerals olivine, feldspar, orthopyroxene and clinopyroxene. In addition calculations are also done for the case of meteorite bodies of the above sizes and having H chondrite and L chondrite compositions. These production rates are compiled in table 6 and table 7 respectively.

The surface production of ^{15}N in the case of any mineral (with oxygen abundance 45%) increases as the size of the body increases and this increase in followed by a decrease in production rate beyond a certain size. The ^{15}N production systematics for the major silicate minerals inside meteorites are as follows. In the case of a meteorite body with radius 18 g/cm^2 the surface production of ^{15}N is 681 atoms/min/kg which increases to 736 atoms/min/kg for a body of radius 72 g/cm^2 and then decreases

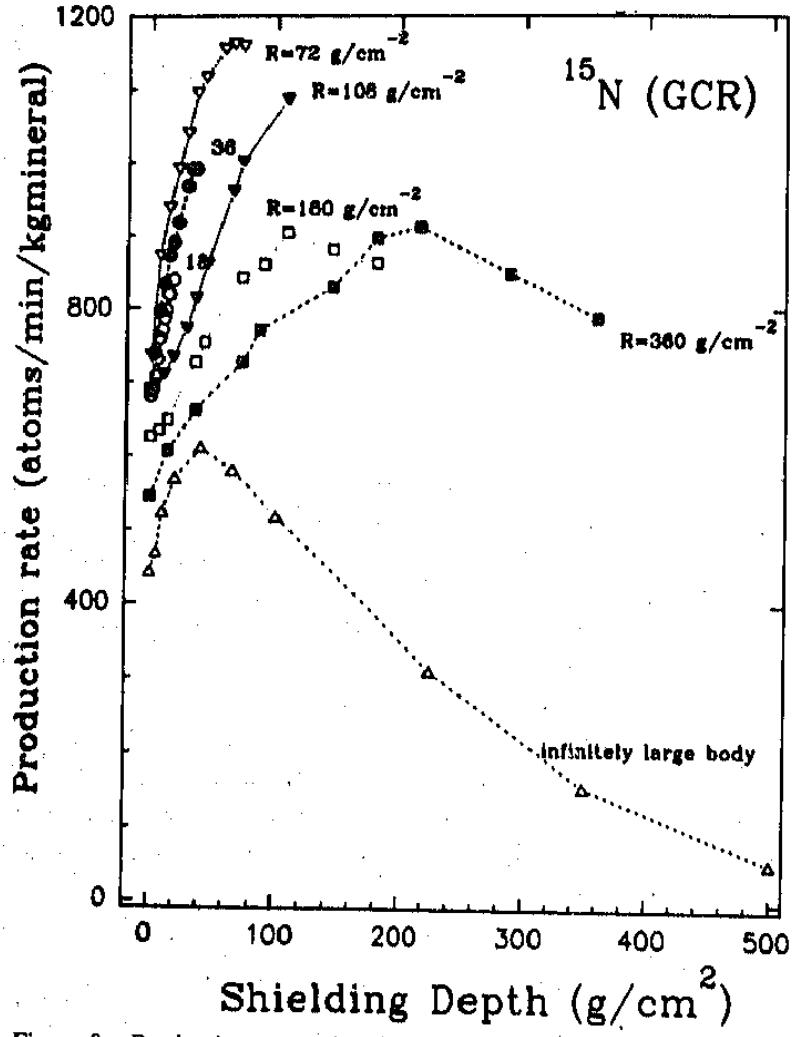

Figure 8. Production rate of GCR produced ^{15}N as a function of shielding depth in meteoroid bodies of various sizes.

with further increase in body size. Considering the depth variation of production rate, the production rate increases with shielding depth inside the meteorite body for meteorites of all sizes as shown in figure 8. The increase is the maximum for the case of a meteorite with radius around 72 g/cm^2 in which case the centre production rate is 1159 atoms/min/kg compared to the surface production rate of 736 atoms/min/kg. Figure 8 shows the ^{15}N production as a function of shielding depth in meteorite bodies of sizes ranging from 18 g/cm^2 to 360 g/cm^2. The production profile for an infinitely large body is also included for purposes of comparison.

The ^{21}Ne production rate varies significantly as the chemical composition of the body changes. These changes are due to the fact that the target element abundances for this isotope change considerably from meteorite of one kind to another and also from one mineral to another. The depth dependence of the production of ^{21}Ne also depends on the main target element from which this isotope is produced. For an olivine inside a body of radius 18 g/cm^2 the surface production of ^{21}Ne is 120 atoms/min/kg and in the case of feldspar the surface production rate is 94 atoms/min/kg. For olivine and feldspar inside a body of size 72 g/cm^2 the surface and center production rates are, respectively, 129 atoms/min/kg and 317 atoms/min/kg (olivine) and 99 atoms/min/kg and 136 atoms/min/kg (feldspar). The surface as well as the center production rates decrease as the size of the body is further increased.

The ^{21}Ne production rates for ortho or clinopyroxene in meteorite bodies having sizes discussed above fall in the range between olivine and feldspar minerals. The depth variations in these cases are similar to that for olivine mineral. Among the two minerals orthopyroxene and clinopyroxene the orthopyroxene values are closer to that of the olivine mineral in bodies of the same size; and the clinopyroxene values are much less compared to the olivine case. The depth variations in both cases are similar to that of olivine. Since the major targets for the production of ^{21}Ne are the same in all these three minerals but their abundance varies, this kind of systematics in the production rates is not surprising.

We have also calculated the production rates of the isotopes ^{14}N, ^{15}N and ^{21}Ne in H and L chondrites. In the case of these two bodies the oxygen abundances used are, respectively, 35·7% for H chondrites and 37·7% for L chondrites. These compositions are adopted from Mason (1979). The ^{15}N and ^{21}Ne productions in L chondrites are higher than the corresponding H chondrite values. The systematics in the depth variation in the production of these isotopes remain the same for the minerals olivine, orthopyroxene and clinopyroxene, described above. The surface production rate of ^{15}N in an L chondrite body of $R = 18$ g/cm^2 ($R = 5$ cms, $\rho = 3{\cdot}6$ g/cm^3) is 570 atoms/min/kg in comparison to the H chondrite value of 541 atoms/min/kg. The center production rate in the case of an L chondrite body of size 18 g/cm^2 is 704 atoms/min/kg. Both the surface production rate and the center production rate increase as the size of the meteoroid is increased to 72 g/cm^2. The surface and center production rates for an L chondrite of this size are 616 and 920 (in units of atoms/min/kg). Further increase in the size of the meteoroid results in a decrease of both the surface and center production rates. For example, in the case of a meter sized L chondrite body ($R = 360$ g/cm^2) the surface and center production rates are (in units atoms/min/kg) 458 and 662.

Now let us have a look at the variations in the cosmogenic ^{15}N/^{21}Ne ratios in meteoroid bodies. In the case of meteoroids of small size ($R = 5$ cm or 18 g/cm^2) there is not much variation in the ^{15}N/^{21}Ne ratio between the surface and the center of

the body. As the size of the meteoroid increases the variations in the $^{15}N/^{21}Ne$ become more pronounced. Consider olivine and feldspar minerals. Values of the ratio $^{15}N/^{21}Ne$ at surface and center for olivine are 5·6 and 4·0, for a body of size 36 g/cm^2. For feldspar mineral the corresponding values are 7·3 and 8·0. In the case of olivine mineral the $^{15}N/^{21}Ne$ ratio decreases and for a feldspar body the $^{15}N/^{21}Ne$ ratio increases from surface to center of the meteoroid. Figures 9(a–d) show the variation in $^{15}N/^{21}Ne$ as a function of shielding depth inside meteoroids of size 18 g/cm^2, 36 g/cm^2, 72 g/cm^2, 108 g/cm^2, 180 g/cm^2 and 360 g/cm^2. The corresponding values for an infinitely large body are also plotted for purposes of comparison. In the case of a meter sized meteoroid the center production ratio of $^{15}N/^{21}Ne$ is half of the surface value of 5·8 for olivine whereas for feldspar the center and surface values of $^{15}N/^{21}Ne$ are 10·7 and 7·6 in the same sized body. The minerals orthopyroxene and clinopyroxene behave in much the same fashion as olivine.

For H and L chondrite bodies of small size ($R = 18$ g/cm^2) the surface and center values of the $^{15}N/^{21}Ne$ production ratio remain the same. For large meteoroids, both of H and L type, the $^{15}N/^{21}Ne$ ratio decreases with shielding depth inside the meteoroid.

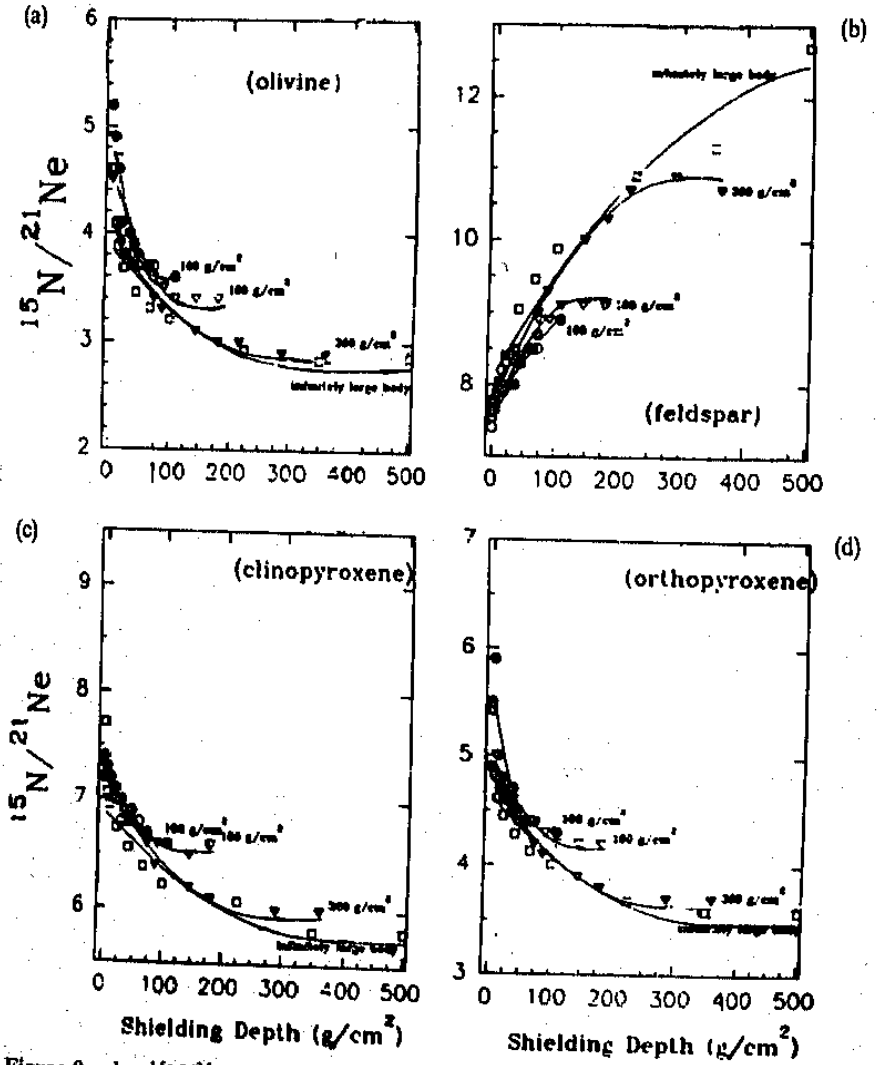

Figure 9a–d. $^{15}N/^{21}Ne$ (GCR) as a function of shielding depth in minerals olivine, feldspar orthopyroxene and clinopyroxene for meteoroid bodies of various sizes.

The surface and center production ratio of $^{15}N/^{21}Ne$ in the case of an L chondrite body of $R = 360\,g/cm^2$ are 6·4 and 3·6.

4.4 *Uncertainties in ^{15}N production rates*

Two factors that influence the production rate of ^{15}N in a sample are the oxygen abundance and the excitation function. Our assumption of ~45% oxygen for all silicate minerals might have an uncertainty of upto 5% for specific cases. This will directly translate into an uncertainty of 5% in the production rate. A more serious ambiguity might still be from the excitation functions. Here again the effect might not be very significant for the SCR production rates wherein only the proton reaction channels need be considered. In the case of GCR production where the secondary particles play an important role, our approach of treating p and n induced reactions to be the same at higher energies, might contribute a larger share to the overall uncertainty in the production rates.

A calibration of these calculated production profiles against measurements in well documented meteorite samples will help in a quantitative assessment of the uncertainties in these production rates. In the case of the aubrite Norton County with well defined trapped nitrogen ($\delta^{15}N = -33‰$) an experimental determination of cosmogenic ^{15}N was feasible (Murty and Varun Sheel 1991). The cosmogenic ^{15}N and ^{21}Ne amounts in this meteorite were (in ccSTP/g units) $^{15}N = 236 \times 10^{-8}$ and $^{21}Ne = 62 \times 10^{-8}$, yielding $^{15}N/^{21}Ne = 3{\cdot}8$. From the bulk composition of Norton County (Walters and Prinz 1979) and the present production rates we derive a value of $^{15}N/^{21}Ne = 3{\cdot}3$, for a sample at 40 g/cm^2 depth. Considering the uncertainties involved in the sample depth, the agreement with the experiment is very good. For a more thorough evaluation, an experimental depth profile of ^{15}N needs to be obtained and such measurements are currently in progress.

5. Conclusions

We have evaluated the production rates of nitrogen and neon isotopes in lunar surface material and in meteoroids of different sizes. These production rates are better estimates, since the cross section data for the production of these isotopes from their cosmochemical targets have undergone major changes in the last couple of years as a result of the recent irradiation experiments and these cross section data are incorporated in the present study.

We observe that the cosmogenic production ratio of $^{15}N/^{21}Ne$ changes with shielding depth in the irradiated body and also that this ratio is significantly different for the low energy SCR and high energy GCR particle irradiations. These differences can be used to differentiate between these two irradiations.

Acknowledgements

We thank Prof. N Bhandari for providing the computer code and valuable suggestions to improve the presentation. Prof. M N Rao has provided a critical review which resulted in clarifying many points.

References

Allen R O Jr and Mason B 1973 Minor and trace elements in some meteoritic minerals; *Geochim. Cosmochim. Acta.* 37 1435–1456

Audouze J, Epherre M and Reeves H 1967 Survey of experimental cross sections for proton induced spallation reactions in He^4, C^{12}, N^{14} and O^{16}, In *High energy nuclear reactions in Astrophysics* (ed.) B S P Shen (New York: W. A. Benjamin) pp. 255–271

Baros F and Regneir S 1984 Measurement of cross sections for ^{22}Na, $^{20-22}Ne$ and $^{36-43}Ar$ in the spallation of Mg, Al, Si, Ca and Fe. Production ratios of some cosmogenic nuclides in meteorites; *J. Phys. (Paris)* 45 855–861

Becker R H, Clayton R N and Mayeda T K 1976 Characterisation of lunar nitrogen components; *Proc. Lunar Sci. Conf. 7th* 1 441–458

Bhandari N 1988 Cosmic ray production rates of neon isotopes in meteoritic minerals; *Proc. Indian Acad. Sci. Earth Planet. Sci.* 97 117–125

Bhandari N and Potdar M B 1982 Cosmogenic ^{21}Ne and ^{22}Ne depth profiles in chondrites; *Earth Planet. Sci. Lett.* 58 116–128

Bhattacharya S K, Goswami J N, Gupta S K and Lal D 1973 Cosmic ray effects induced in a rock exposed on the moon or in free space: contrast in patterns for 'tracks' and 'isotopes'; *Moon* 8 253–286

Caffee M W, Hohenberg C M, Nichols Jr R H, Olinger C T, Wieler R, Pedroni A, Signer P, Swindle T D and Goswami J N 1991 Do meteorites contain irradiation records from exposure to enhanced activity sun?; In *The sun in time* (eds) C P Sonett, M S Giampapa and M S Matthews (University of Arizona Press) pp. 413–425

Grady M M, Wright I P, Carr L P and Pillinger C T 1986 Compositional differences in enstatite chondrites based on carbon and nitrogen stable isotope measurements; *Geochim. Cosmochim. Acta.* 50 2799–2813

Guzik T G, Wefel J P, Crawford H J, Greiner D E, Lindstorm P J, Schimmerling W and Symons T J M 1985 Implications of new measurements of $^{16}O + p \rightarrow {}^{12,13}C, {}^{14,15}N$ for the abundances of C, N isotopes at the cosmic ray source; *Proc. 19th Internat. Cosmic Ray Conf. La Jolla* 2 80–82

Hohenberg C M, Marti K, Podosek F A, Reedy R C and Shirck J R 1978 Comparison between observed and predicted cosmogenic nobel gases in lunar samples; *Proc. Lunar Planet. Sci. Conf.* 9th 2311–2344

Honda M 1988 Statistical estimation of the production of cosmic-ray-induced nuclides in meteorites; *Meteoritics* 23 3–12

Lavielle B, Sanvageon H, Bertin P and Haouat G 1990 Cross sections of neon isotopes induced by 5, 7, 16 and 19 MeV neutrons; *Phys. Rev.* C42 305–308

Leich D A, Borg R J and Lanier V B 1984 Production rates of neon and xenon isotopes by energetic neutrons; *Workshop on cosmogenic nuclides, Los Alamos National Laboratory, New Mexico*, pp. 22–24

Mason B 1979 Cosmochemistry, Part I, Meteorites; In Data of geochemistry (ed) M Fleischer (Washington: Geol. Surv. Prof. Paper) 440 B1–B132

McKibben R B, Pylee K R and Simpson J A 1982 The galactic cosmic ray intensity gradient and large scale modulation in the heliosphere; *Astrophys. J.* 254 L23–L27

Michel R, Dragovitsch P, Cloth P, Dagge D and Filges D 1991 On the production of cosmogenic nuclides in meteoroids by galactic protons; *Meteoritics* 26 221–242

Murty S V S and Marti K 1990 Search for solar-type nitrogen in the gas rich pesyanoe meteorite; *Meteoritics* 25 227–230

Murty S V S and Goswami J N 1992 Nitrogen, noble gases and nuclear tracks in lunar meteorites MAC 88104/105; *Proc. Lunar Planet. Sci.* 22 225–237

Murty S V S and Varun Sheel 1991 Production rate of cosmogenic nitrogen from Norton County aubrite (abstract); *Meteoritics* 26 375

Murty S V S 1990 Cosmogenic nitrogen in Kapoeta: an attempt to isolate solar cosmic ray produced component; *Lunar Planet. Sci. XXI* 1 829–830

Olson D L, Bermann B L, Greiner D E, Heckman H H, Lindstorm P J and Crawford H J 1983 Factorisation of fragment production cross sections in relativistic heavy ion collisions; *Phys. Rev.* C28 1602–1613

Potdar M B and Bhandari N 1979 Natural radioactivity of Luna 24 and Apollo -16 soils; *Proc. Indian Natl. Sci. Acad.* A45 32–38

Rao M N, Garrison D H, Bogard D D and Reedy R C 1993 Solar-flare implanted $^4He/^3He$ and solar-proton produced Ne and Ar concentration profiles preserved in Lunar rock 61016; *J. Geophys. Res.* 98 7827–7835

Read S M and Viola Jr V R 1984 Excitation functions for A $\geq$ 6 fragments formed in ^{1}H and ^{4}He induced reactions on light nuclei; *At. Data Nucl. Data Tables* **31** 359–397

Reedy R C 1981 Cosmic-ray-produced stable nuclides: various production rates and their implications; *Proc. Lunar Planet. Sci.* **B12** 1809–1823

Reedy R C and Arnold J R 1972 Interaction of solar and galactic cosmic ray particles with the moon; *J. Geophys. Res.* **77** 537–555

Reedy R C 1983 Nuclide production by primary cosmic rays in very small objects (abstract); *Meteoritics* **18** 383–384

Reedy R C 1985 A model for GCR particle fluxes in stony meteorites and production rates of cosmogenic nuclides; *Proc. Lunar Planet. Sci. Conf. J. G. R.* **C90** supplement C722–C728

Reedy R C 1992 Solar-proton production of neon and argon; *Lunar Planet. Sci. Conf. XXII* 1133–1134

Reedy R C, Herzog G F and Jessberger E K 1979 The reaction Mg(n, α) Ne at 14·1 and 14·7 MeV: cross sections and implications for meteorites; *Earth Planet. Sci. Lett.* **44** 341–348

Shapiro M M and Silberberg R 1970 Heavy cosmic ray nuclei; *Annu. Rev. Nucl. Sci.* **20** 323–392

Sisterson J M, Jull A J T, Donahue D J, Koehler A M, Reedy R C and Engelhardt 1991 Cross sections for production of carbon 14 from oxygen and silicon: Implications for cosmogenic production rates; *Meteoritics* **26** 395–396

Walters T R and Prinz M 1979 Aubrites: Their origin and relationship to enstatite chondrites; *Proc. Lunar Planet. Sci. Conf.* **10** 1073–1093

Webber W R, Braugigam D A, Kish J C and Schrier D A 1983 Fragmentation of 500 MeV/Ne and O nuclei in CH_2, C and H targets – Charge and isotopic composition; *Proc. 18th Intl. Cosmic Ray Conf., Bangalore* **2** 202–205

Webber W R, Kish J C and Schrier D A 1990 Formula for calculating partial cross sections for nuclear reactions of nuclei with $E \geq 200$ MeV/nucleon in Hydrogen targets; *Phys. Rev.* **C41** 566–570